Qeios

Modeling and Analysis of Phase-locked loops: a non reductionist approach

José Roberto C. Piqueira*, Felipe Freitas and
Luis Antonio Aguirre****

Abstract Phase-locked loop (PLL), conceived in 1932 by H. Bellescize, has been the basic electronic component in the development of communication technology from the early analog radio receptors to modern digital civil and military facilities. Traditionally, the analysis is conducted by modeling the dynamical behavior of phase and frequency errors, hence following a phase reduction approach. One of the main goals of the present work is to describe and investigate the dynamics of a PLL node by representing it in full state-space, here called non reductionist model, without the usual design simplifications i.e., considering different input and output frequencies and not neglecting the higher frequencies components generated in the phase detection process. On the one hand, this approach complicates the use of analytical tools but on the other hand it permits an efficient numerical approach that can be used for precise definition of regions in parameters space that show the boundaries between synchronization and non synchronization regimes, even when noise is considered. Results show that the PLL node can be simulated in a more realistic way using the state-space model and that a number of design-relevant aspects can now be investigated numerically.

Keywords bifurcation; dynamics; parameter space; phase error; synchronization.

PACS 02.30.Oz; 02.60.Cb

*Escola Politécnica da Universidade de São Paulo
Avenida Prof. Luciano Gualberto, travessa 3, n. 158, 05508-900
São Paulo - SP, Brasil
Tel.: 55 11 3091 5647
E-mail: jose.piqueira@usp.br
** Universidade Federal de Minas Gerais
Av. Antônio Carlos 6627, 31270-901
Belo Horizonte - MG, Brasil
E-mail: aguirre@ufmg.br

1 Introduction

The phase-locked loop (PLL) architecture proposed for frequency demodulation in the 1930's [1] has been a paradigm for designing a large spectrum of electronic and communication synchronization strategies, being present in the new generation of wireless devices and dense communication networks [2,3]. Generally being an anonymous element, the PLL is a vital element to detect clock signals providing synchronization for circuits, devices and networks. Despite miniaturization, the original circuit architecture remained almost unchanged although it improved significantly with digital signal processing. Such improvement allows accurate and precise operation over a very broad frequency band. Faster communications and geographical localization are strongly dependent of how clock signals are distributed and detected. This requires parameter values that take into account nonlinearities either for the whole network or the interconnected nodes.

Rigorous analytical and practical studies about isolated PLLs [4] and their behavior when connected forming networks [5,6] revealed that despite all the complexity, PLL digital networks are efficient and capable of changing our daily life [7].

Contemporarily, some seminal works appeared [2,3], presenting mathematical formulations and results regarding the behavior of the parameters of the entire network, which served as basic references to the subsequent important developments in communication structures. Currently, such developments are being used with design tools and complemented by the analysis of parameter variations [4].

In this context, the models were developed in a simplified way, considering that the two signals to be synchronized present almost the same frequency with the terms of phase differences responsible for the error to be corrected to align the local clock signal with the input coming from a remote device or network node [8,9]. In such models, the PLL order is defined as one plus the order of the low-pass filter implemented in the loop [9] and in this work such a nomenclature is maintained.

Usually, synchronization systems present acceptable performance when second-order PLLs, i.e. with first-order loop filters, are used as network nodes [10]. However there are some situations where more accurate transient responses are needed, demanding second-order loop filters, resulting in third-order PLLs [11].

In such cases, the design must take into account possible instabilities [11] and, depending on parameter values, Hopf bifurcation and chaotic behaviors can appear [12].

Unfortunately, phase reductionistic models [13] are not generally effective to choose design parameters because they do not take into account the high frequency components present at the low pass filter output even in the second-order case [14] because the filter is considered to be ideal.

Understanding the filter operation in a more realistic way is one of the main motivations to develop a state-space model for the PLL operation. Other motivations for the non reductionist model include i) being able to simulate state variables compatible with measurable magnitudes in real circuits, hence frequency and phase detection processes can be accurately related to filter parameters; ii) the state space model is valid even for large phase errors; and iii) it enables the designer to investigate the

effect of noise that may appear in different points of the system. This is a significant advantage over the reductionist model, which is generally noise-free.

This paper aims at investigating dynamical aspects related to synchronization performance and possible de-synchronization of third-order phase-locked loops (PLL) due to parameters variations.

The model representing the third-order PLL is actually a fourth-order state-space model where no state variable is the phase, rather the phase must be estimated from the oscillating signals produced by the PLL components. The state-space model comes much closer to the circuit implementation of a practical PLL and therefore becomes an important tool for design of such systems.

A PLL (Fig. 1) is composed of a phase detector (PD) where the input signal, $u(t)$, and the voltage controlled oscillator (VCO) feedback output, z_1, are added and multiplied by a gain K_d, resulting the filter input v_d.

The low-pass filter (LPF) with transfer function $F(s)$ attenuates high-frequency components, generating the VCO control input v_c that adjusts the VCO whole phase, considering that its free-running angular frequency is ω_0, with gain K_v.
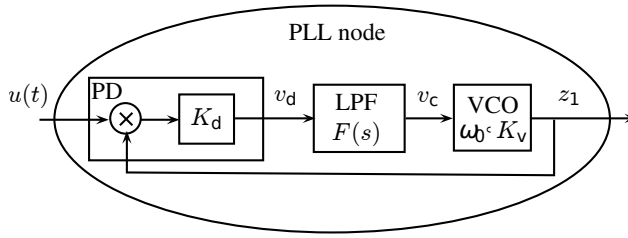
Fig. 1 Block diagram of non-reductionist version of a PLL node. The $u(t)$ and the node output z_1 are multiplied.

The paper is organized as follows. In Section 2, a state space model is studied, with the classical basic topology of a PLL (Fig. 1) used to write the state equations. It is shown that the local phase PLL model complements the corresponding reductionist version, reviewed in [15], allowing to access the time evolution of the main signals, as illustrated with an example. To study how the constitutive parameters of the blocks affect the synchronization performance, several examples discussed in Sec. 3 confirm the effective contribution of this approach to give a global view of how node parameters affect the synchronization performance. Although the presented approach is analytically complicated when compared to the traditional model, it permits a simple and accurate numerical simulations, even considering noise, as exemplified in Section 4. Section 5 completes the work with the main conclusion and discussions on how the developed results can be used according to particular specifications of a design task.

1.1 Contributions

The main contribution is the proposition and numerical analysis of a full state-space model instead of the usual phase reduction model [13], here called a reductionist model. The state-space formulation of the PLL node contributes in the design of synchronization systems because

– nonlinear effects of phase-detection are taken into account;
– state-space variables are directly related to measurable circuit accessible points;
– non-ideal filter effects are considered and high frequency disturbances can be evaluated;
– noise effects can be considered in a friendly way;
– adequate parameter regions can be estimated, even for a high order filtering process.

2 State space model

Consider the PLL node shown in Fig. 1. The starting point is to write the equation for an oscillator:

$$\begin{cases} \dot{z}_1 = z_2 \\ \dot{z}_2 = -\omega_{inst}^2 z_1, \end{cases} \tag{1}$$

which has solution $z_1 = A\cos\omega_{inst}t$, where A is a constant that depends on initial conditions and ω_{inst} is the instant frequency. A key device in a PLL is the voltage controlled oscillator (VCO). In order to represent a VCO it suffices to write the instant frequency as:

$$\omega_{inst}(t) = \omega_0 + K_v v_c(t), \tag{2}$$

where ω_0 is the central frequency, K_v is the VCO gain and $v_c(t)$ is the corresponding input voltage, therefore $z_1 = A\cos[\omega_0 + K_v v_c(t)]t$, from where it is seen that the frequency of the VCO given by (1)-(2) depends on $v_c(t)$.

It is commonplace to normalize the frequency by choosing ω_0=1 rad/s. Therefore the VCO can be interpreted as implementing a frequency modulated output $z_1(t)$ with carrier ω_0 and modulating signal $v_c(t)$.

The voltage $v_c(t)$, in turn, is the output of a linear filter, as for instance

$$F(s) = \frac{V_c(s)}{V_d(s)} = \frac{b_1 s + b_0}{s^2 + a_1 s + a_0}, \tag{3}$$

where $V_c(s)$ and $V_d(s)$ are, respectively, the Laplace transforms of $v_c(t)$ and $v_d(t)$ which is the output of the *phase detector* (PD).

$F(s)$ can be realized as

$$\begin{cases} \dot{x}_1 = x_2 \\ \dot{x}_2 = -a_0 x_1 - a_1 x_2 + v_d(t), \end{cases} \tag{4}$$

with output given by $v_c(t) = b_0 x_1 + b_1 x_2$.

Clearly, many other filter structures can be used and since all that is required in the end is to have the corresponding state space realization, the proposed model can easily accommodate nonlinear filters.

Finally, the phase detector is modeled as the product of the VCO output and the "node input", $u(t)$. Hence

$$v_{\mathrm{d}}(t) = K_{\mathrm{d}}z_1(t)u(t),\tag{5}$$

where the constant K_{d} is the PD gain.

The final model in state space is:

$$\begin{cases}\dot{x}_1 = x_2 \\ \dot{x}_2 = -a_0 x_1 - a_1 x_2 + K_{\mathrm{d}}z_1 u(t) \\ \dot{z}_1 = z_2 \\ \dot{z}_2 = -[\omega_0 + K_{\mathrm{v}}(b_0 x_1 + b_1 x_2)]^2 z_1,\end{cases}\tag{6}$$

with node input $u(t)$ and node output $z_1(t)$. The second and the forth equations of (6) reveal that the node is nonlinear.

As with the physical oscillators, all the state variables are oscillating signals, that is, none of them is explicitly the output or input phase, as usually considered. This brings the simulation closer to a practical situation but at the cost of a more elaborate simulation and a clear increase in the difficulty of developing any analytical results.

To take $z_1(t)$ as the output is equivalent to use the simple measuring function $h(\boldsymbol{x}) = z_1(t)$, where $\boldsymbol{x} \in \mathbb{R}^4$ is the state vector. In Example 1 it will shown that other measuring functions can be used as, for instance, $h(\boldsymbol{x}) = \psi_{\mathrm{o}}(t)$, where $\psi_{\mathrm{o}}(t)$ is the output phase.

Example 1 This example aims at validating model (6) via numerical integration using a fourth-order Runge-Kutta with fixed integration interval of $\delta_t = 0.01$. The other parameters used were: $a_0=1/3$, $a_1=1/2$, $b_0=1/3$, $b_1=1/12$, that is

$$F(s) = \frac{s + 4}{12s^2 + 6s + 4},\tag{7}$$

after simple adjustments. The frequency response $F(j\omega)$ is shown in Figure 2. The gains were taken as $K_{\mathrm{d}}=K_{\mathrm{v}}=0.7$ and $\omega_0=1$ rad/s. The input was $u(t)= \sin(1.02t)$ and the initial conditions were taken from a zero-mean Gaussian distribution with variance $\sigma^2=0.01$. It should be noticed that a slight mismatch between input frequency and the VCO central frequency ω_0 was considered.

The filter input $v_{\mathrm{d}}(t)$ and output $v_{\mathrm{c}}(t)$ are shown in Figure 3. The effect of the low pass filter is clear from this figure. It should be noticed that $v_{\mathrm{c}}(t)$ oscillates instead of being a dc signal as assumed in the context of reductionist models [15].

To improve filter performance one could reduce the filter bandwidth or increase the roll-off rate by adding more poles to $F(s)$. The latter alternative is likely to improve the filter performance but also to deteriorate the PLL performance as the increase of phase-lag in the loop is known to be deleterious.

The VCO output is shown in Figure 4. The central frequency of this signal is ω_0 and is roughly half of the high-frequency component of the signal in Figure 3.
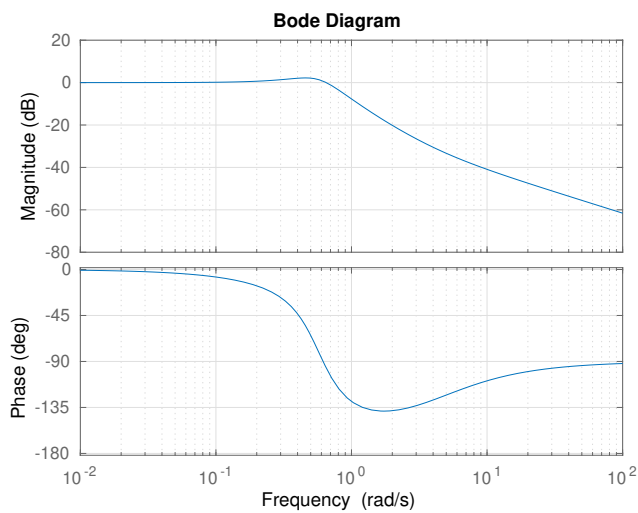
Fig. 2 Frequency response of the low pass filter in (7).
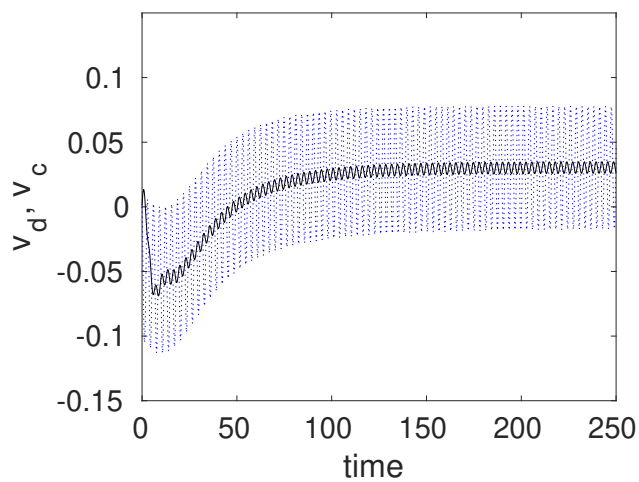
Fig. 3 The filter input $v_d(t)$ is shown in dotted blue lines. This has slow- and high-frequency components. The filter output $v_c(t)$ is indicated in a solid black line and shows that whereas the high-frequency component is greatly attenuated the it is not completely eliminated as assumed in the reductionist model.

The question now is how does the phase of the VCO output $z_1(t)$ relate to that of the input signal $u(t)$.

In order to answer this question, Figure 5 shows a Lissajous plot. If the signals were identically synchronized, this plot would be a diagonal line. If the signals are phase synchronized, then the result is an ellipse where the width corresponds to the phase difference
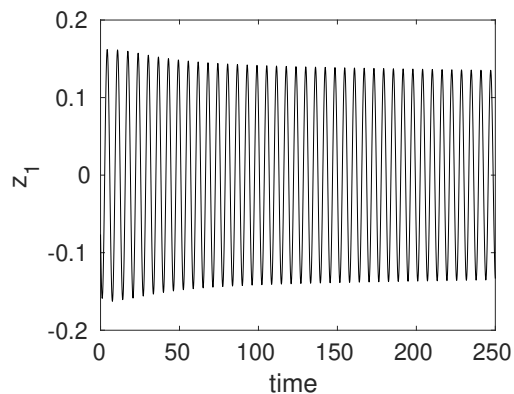
Fig. 4 VCO output when the input is solid black line in Figure 3.

If the phases difference is constant the result is a single ellipse. In Figure 5 there are regions in which the line is slightly thicker indicating that the relative phase has a small fluctuation.
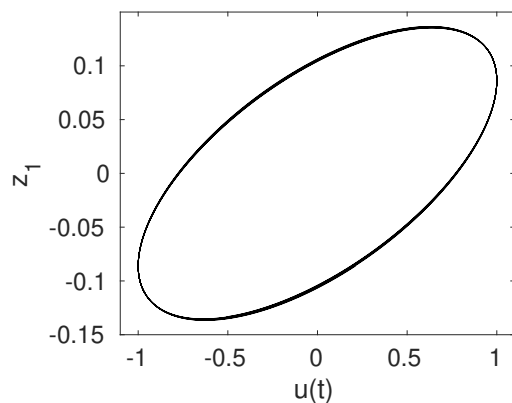
Fig. 5 This Lissajous plot suggests that the relative phase is nearly constant.

In many problems it is important to have an estimate of the phase. In the case of the input $u(t) = \sin(1.02t)$, because it is sinusoidal, the phase is simply $\psi_i(t) = 1.02t$. In the case of the VCO output, a convenient way of estimating the phase is:

$$\psi_o(t) = \tan^{-1}\left(\frac{z_2}{z_1}\right), \tag{8}$$

which is in the form of a measuring function $h(\boldsymbol{x}) = \psi_o(t)$. A relative phase can be defined as $\theta(t) = e(t) = \psi_i(t) - \psi_o(t)$. Phase locking happens for constant $\theta(t)$, and the condition for phase synchronization, which is more relaxed, is $\theta(t) < C$, where C is a constant usually smaller than 2π.

Figure 6 shows the first difference of the relative phase, that is, $e(t) - e(t-\delta_t)$, which is an approximation of the derivative of the relative phase.
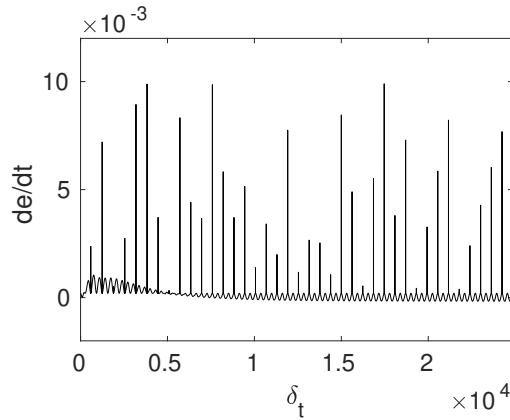
Fig. 6 First difference $e(t) - e(t-\delta_t)$ of the relative phase.

As can be seen from Figure 6 changes in relative phase remain small indicating phase synchronization. The spikes are probably due to the discontinuity of the *atan* function used to compute the phase. Therefore, despite a small mismatch in the frequency of the input signal compared to the central frequency of the VCO, the input and output signals of the node become phase synchronized.   □

Observing the example, non-reductionist strategy to model PLL dynamics provides the possibility of having the temporal evolution of the periodic signals through the loop, complementing the reductionistic strategy that gives only corresponding phase and frequency errors and their trajectory to equilibrium states.

Besides, Figures 4, 5, and 6 show signals that have counterparts in real electronic circuits, differently from the reductionist strategy where instead of voltage signals they directly provide the phase error.

3 Performance of the PLL node

To investigate the performance of the PLL node as it tries to synchronize to the node input $u(t) = \sin \omega_i t$, the node phase is computed using equation (8), as shown in the next example.

Example 2 Using the same filter as for Example 1 and the additional parameters: $\omega_i = 1.001$ rad/s and $\omega_0 = 1.002$ rad/s, $\delta_t = \pi/300$, $K_d = K_v = 0.8$, the VCO is simulated with (2) and with an integral term

$$\omega_{\text{inst}}(t) = \omega_0 + K_v v_c(t) + K_i \int_0^t v_c(\tau)\mathrm{d}\tau, \tag{9}$$

with K_i=0.5. It should be noticed that the inclusion of the integral term in (9) would not be straightforward in the reductionist model.

The motivation for including the integral term stems from the interpretation of $v_c(t)$ as a proxy for the *frequency* error and from the aim of achieving null steady-state error. The main results are shown below in Figures 7 and 8.
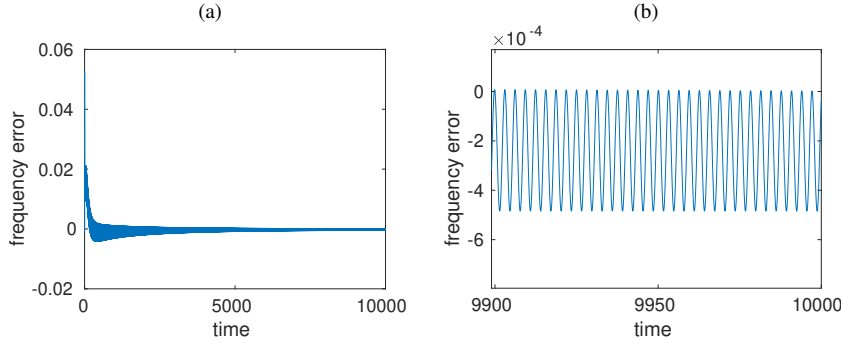
Fig. 7 (a) Frequency error $\omega_i - \omega_{inst}$ over 1,593 revolutions and (b) zoom. The VCO is implemented with (2). Notice that the steady-state error is almost always negative.
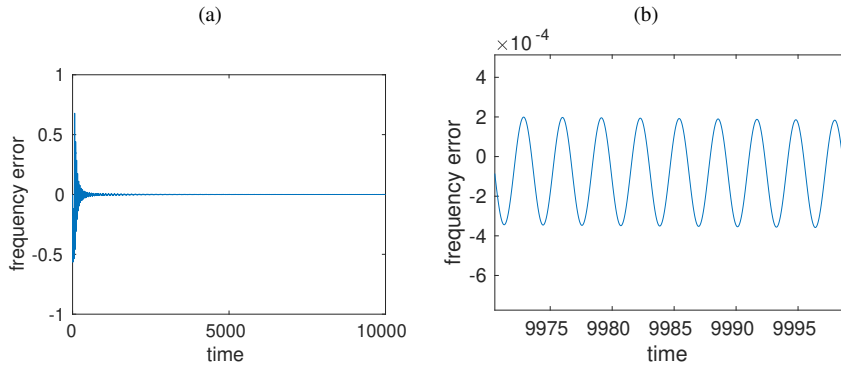
Fig. 8 (a) Frequency error $\omega_i - \omega_{inst}$ over 1,593 revolutions and (b) zoom. The VCO is implemented with (9). Notice that the error mean in steady-state is much closer to zero than for the case in Figure 7.

□

A common approach to determine if synchronization has or not been achieved is to define *ad hoc* thresholds such as [16][p. 82]:

$$\left|1 - \frac{\omega_i}{\Omega_o}\right| < 2 \times 10^{-3};$$
$$|\psi_o(t) - \omega_i t| < K, \tag{10}$$
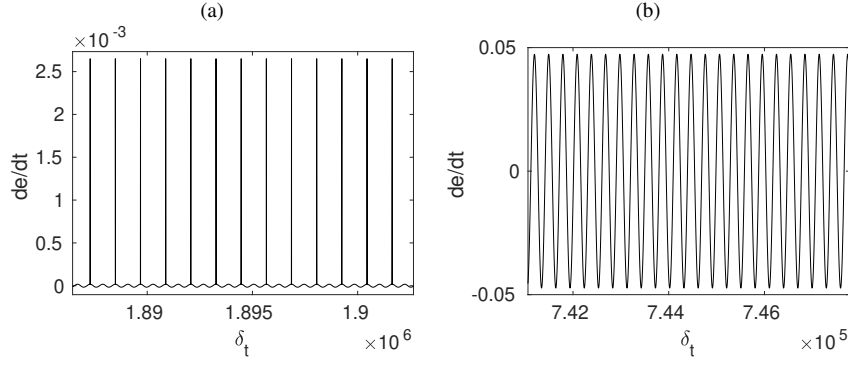
Fig. 9 First difference of phase error computed (a) using $e(t)=\omega_i t - \psi_o(t)$, see (8) and (b) using $e(t)=\omega_i t - \omega_{inst} t$, see (2).

where K is a constant often assumed to be equal to π, $\Omega_o = \langle \omega_o \rangle = \langle \dot{\psi}_o \rangle$ is the average phase growth rate, which can be computed as [16][Eq. 4.46]

$$\Omega_o = \lim_{T \to \infty} \frac{\psi_o(T) - \psi_o(0)}{T}. \tag{11}$$

The second condition in (10) was introduced in [23] and is known as the condition for *phase entrainment*, which is clearly weaker than condition $\psi_o(t) - \omega_i t = K$. *Frequency entrainment* can be tested using the first condition in (10).

In (10) it is common to take $K = \pi$ because when the phases are *not* locked, phase slips of 2π are verified and hence π is sufficiently small to detect such phase slips.

It should be noted that this is true for most reductionist models where stable and unstable fixed points in the phase relative space are separated by π.

In what follows, instead of defining thresholds in an *ad hoc* way, we compute

$$
\begin{aligned}
f &= \left| 1 - \frac{\omega_i}{\Omega_o} \right| ; \\
e &= |\psi_o(t) - \omega_i t| ; \\
m &= \langle |\dot{e}| \rangle ; \\
s &= \text{std}(\dot{e}).
\end{aligned} \tag{12}
$$

In (12), f is a measure of frequency entrainment, e is an estimate of phase error, where $\psi_o(t)$ is computed using (8), m is the time average of $|\dot{e}|$ and s, the standard deviation of $\dot{e}$.

The reason for using time average and standard deviation on the derivative of the phase error is that, due to the fact that here the filtering is *not* assumed to be ideal, the resulting phase derivative has small oscillations. The following example illustrates the use of (12).

Example 3 Here the filter is the same as for Example 1, $\omega_0=1.0$ rad/s, $\delta_t=\pi/300$ and the VCO is simulated with (2) and with an integral term – see (9) – with $K_i=0.22$. The input frequency was varied in the range $0.2 \le \omega_i \le 1.8$ rad/s and the gains were within $0.1 \le K_d=K_v \le 3$, yielding 520 different combinations of ω_i and $K_d=K_v$.

The simulation time for each case was t_f=10000 and the values in (12) were computed in the second half of the data to reduce transient effects. Initial conditions were taken randomly around the origin of the state space. The results are summarized in Figures 10, 11 and 12.

The blue flat floors in Figures 10 and 11 at the orders of 10^{-3} and 10^{-5}, respectively, and correspond to the region in which the PLL node has best performance in terms of phase-synchronizing with the input. Consequently, as the figure shows, determining PLL capture amounts to selecting a combination of parameters that is inside de blue region of the diagrams. This procedure does not require complicated analytical work for the design of higher order synchronization networks [17].

The consistency of the synchronization process can be studied observing Figure 12 which shows that the variability of the absolute phase error derivative is lower when $\omega_i \approx \omega_0$ and gradually increases as ω_i deviates from the VCO central frequency $\omega_0 = 1$ rad/s. Hence whereas Figures 10 and 11 can be used to select parameters that result in synchronization, Figure 12 goes a step further and shows the subregions, within the blue plateau, that result in improved robustness of synchronism.

Beyond the boundary of the blue region the performance of the PLL node degrades abruptly. Roughly the range of values for which good performance is achieved "comfortably" is $0.6 \leq \omega_i \leq 1.5$ rad/s and $1 \leq K_d=K_v \leq 2$.
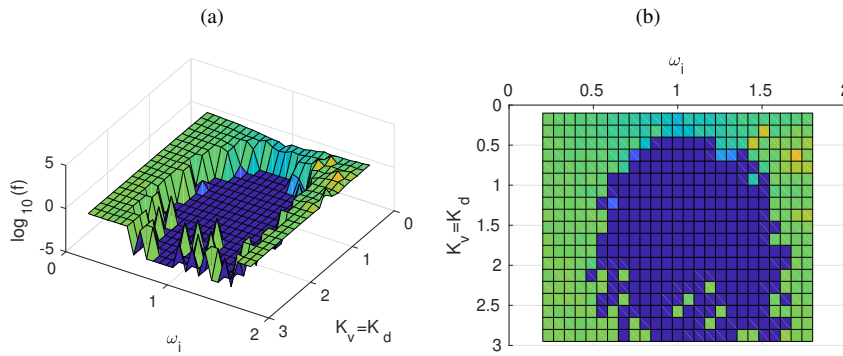
Fig. 10 Logarithm of coefficients in (12) for Example 3. The floor in (a) is at the order of 10^{-3}; (b) 2D top view of (a).

As it can be noticed examining examples 2 and 3, using non reductionist approach to measure PLL performance, despite being analytically complicated, provides a complete idea about capture and lock-in ranges [8, 17] simply observing the permitted synchronization regions of diagrams, allowing to choose gain parameters according to input frequency variations.

Former works faced the problem of determining capture range for third order PLL by using the reductionist model [11, 12, 18] and bifurcation diagrams relating parameters with possible dynamical behaviors. Although such diagrams present results close

(a)   (b)
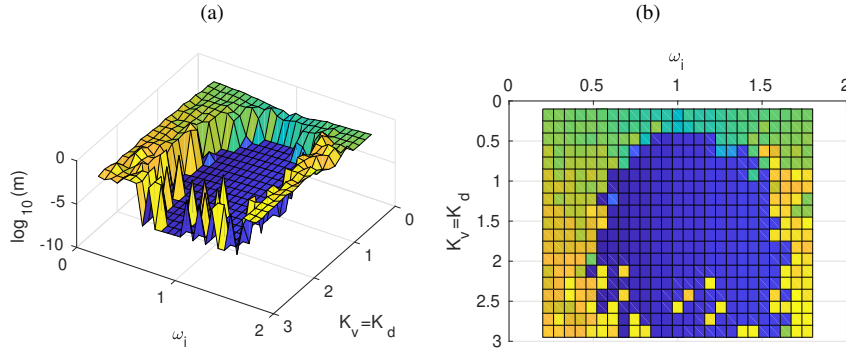
Fig. 11 Logarithm of coefficients in (12) for Example 3. The floor in (a) is at the order of 10^{-5}; (b) 2D top view of (a).

(a)   (b)
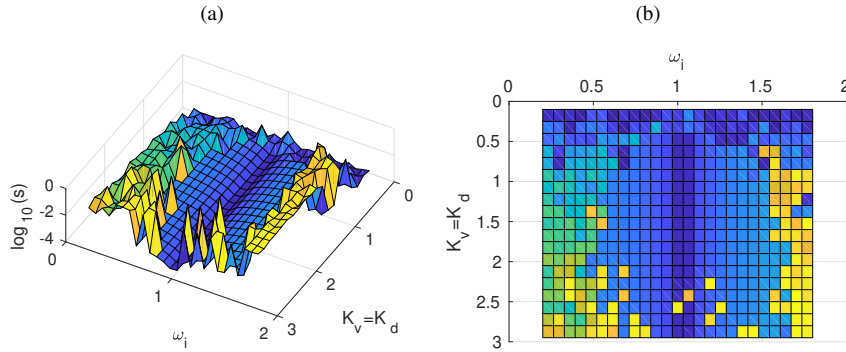
Fig. 12 Logarithm of coefficients in (12) for Example 3. The floor in (a) is at the order of $10^{-3.5}$; (b) 2D top view of (a).

to the ones shown in Figures 10 and 11, Figures 10 and 11 are richer than the ones presented in [11, 12, 18] because the transition zones between behaviors are detailed. Additionally, synchronization quality can be evaluated in Figure 12.

4 Noisy Scenarios

An additional feature of the described non reductionist approach is the capability to determine the capture and lock-in ranges, even in the presence of noise. In the present study noise is added to the VCO central frequency and to the input signal and to see how this affects performance and synchronization boundaries as the gains are varied.

This is illustrated adding noise to some signals in the simulation of the system described in Example 3. The noise was taken from a zero-mean Gaussian distribution, with variance equal to $\sigma^2 = 0.01$ and added to both: the central frequency ω_0 and the input $u(t)$.

The tuning parameters in this case were $K_d = K_v = 0.8$, $K_i = 0$, $\omega_0 = 1$ rad/s. The filter parameters are as before and so was the simulation time $t_f = 10000$.

The initial conditions were taken randomly around the origin of the state space. The values in (12) were computed over the second half of the data. Figure 13 summarizes the results when the noise was added to the VCO central frequency.

As can be seen, the PLL node is quite robust to noise in ω_0 as about 120 out of 200 runs show performance very close to the noise-free case. The worse runs indicated in Fig. 13(a) resulted in a frequency mismatch of about 2.5%. Over 87% of the runs had frequency mismatch less than 1%.
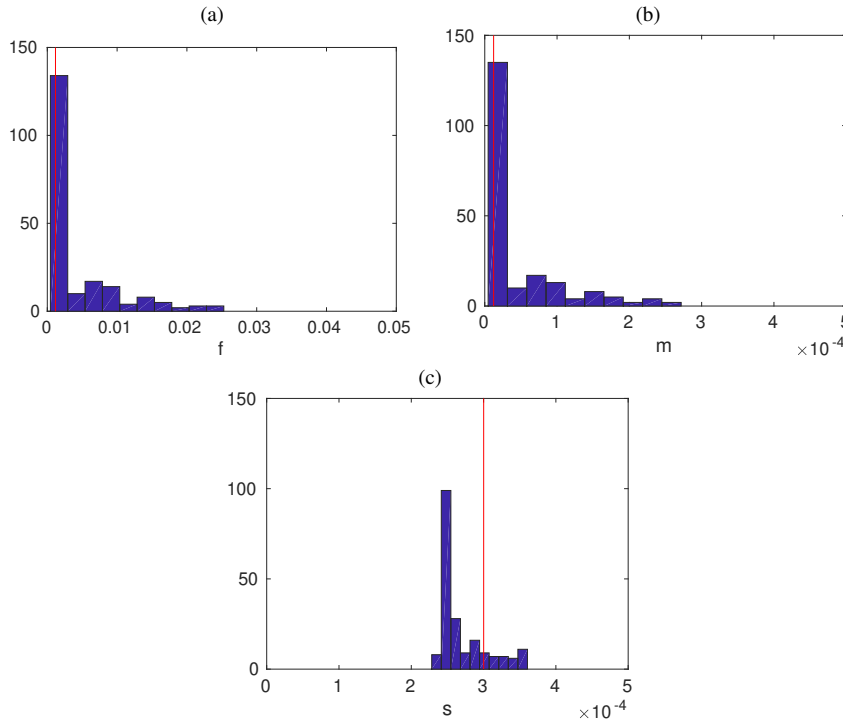
Fig. 13 Histograms of coefficients in (12) for 200 Monte Carlo runs when noise is added to the parameter ω_0. The red vertical lines correspond to the values of (a) f, (b) m and (c) s in the noise-free case.

Figure 14 summarizes the results when the noise was added to the input of the PLL node. As can be seen the robustness in this case is even higher than for noise in the frequency. The distributions are very narrow indeed indicating that the PLL node remains practically unaffected by high-frequency noise in the input.

In the sequel, as done in Example 3, the PLL node was simulated over a grid of 520 combinations of $K_v = K_c$ and ω_i values. This time noise was added simultaneously to both ω_0 and $u(t)$. The results are summarized in Figures 15–17 which should be compared to the noise-free situation, illustrated in Figures 10, 11 and 12. To facilitate comparison such figures will be reproduced side by side with the noisy counterpart.
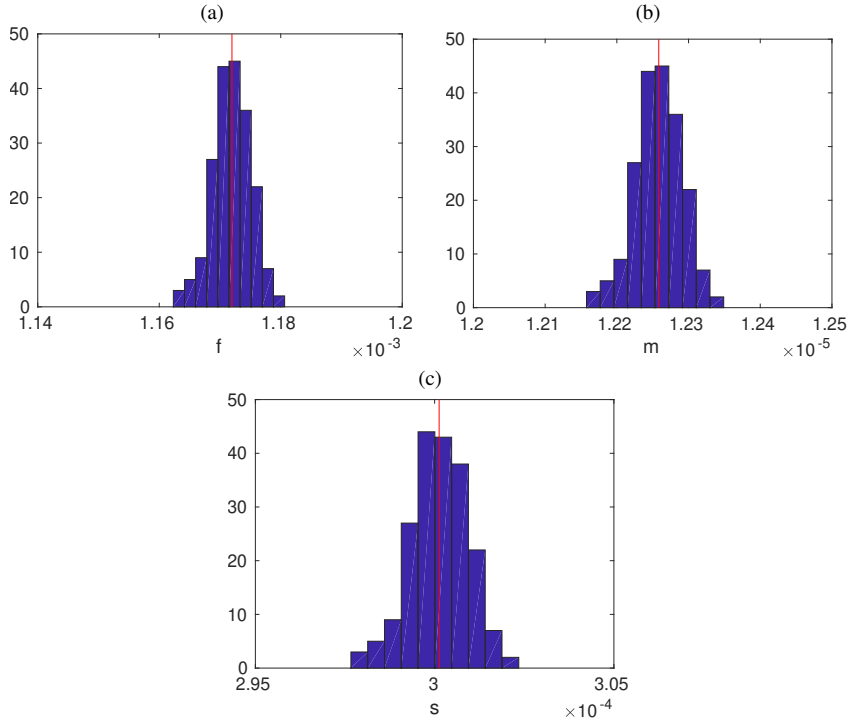
Fig. 14 Histograms of coefficients in (12) for 200 Monte Carlo runs when noise is added to the input signal $u(t)$. The red vertical lines correspond to the values of (a) f, (b) m and (c) s in the noise-free case. Notice that the width of the histograms in this case is much narrower than those in Fig. 13.

As a general remark concerning Figures 15 and 16, it is pointed out that the effect of the noise added simultaneously to ω_0 and $u(t)$ is to reduce the locking region in parameter space $\{K_v=K_c, \omega_i\}$, however whenever synchronization occurs it is of the same quality as for the noise-free case. This is seen by noticing that the level of the floor in such figures has the same order of magnitude as for the noise-free case.

Another interesting remark, which is clearly seen in the 2D projections is that the noise intensifies the asymmetry of the locking region especially along the direction of ω_i. In other words, the presence of noise limits the capacity of synchronization for $\omega_i < \omega_0$.

Hence during design there is a smaller and more asymmetrical region in parameter space that will result in synchronization. In practice this means that the choice of parameters in the noisy case should be done with greater care.

A rather curious phenomenon can be observed in Figure 17, which is a "stabilizing effect" of the noise. Similar situations in other contexts have been reported elsewhere [19]. It should be noticed that the parameter s – see (12) – quantifies the dispersion of values of the phase error derivative. Hence small values of s do not imply synchronization but rather indicate that whatever is the operating condition the corresponding variability is small.
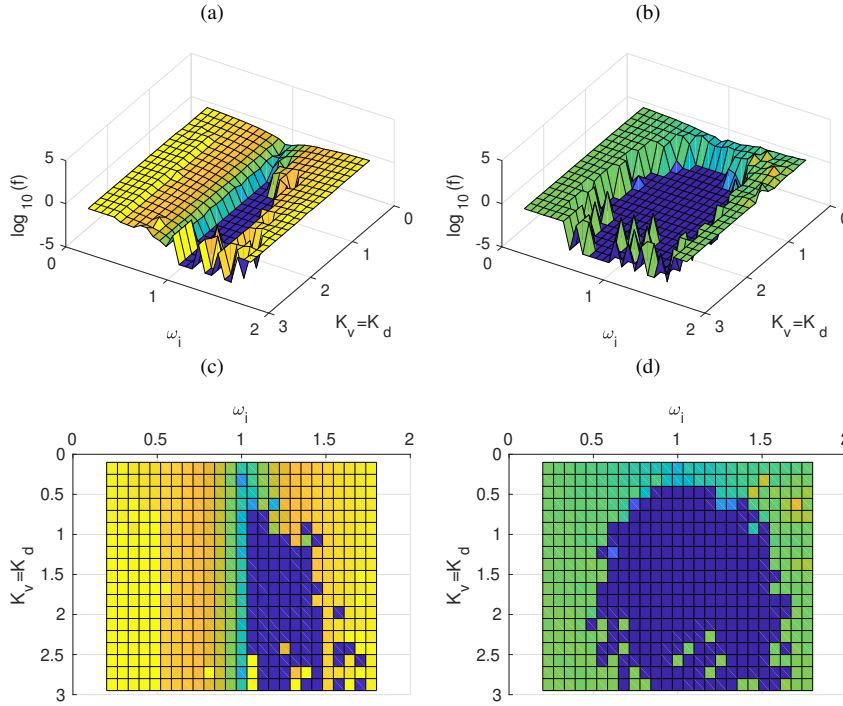
Fig. 15 Logarithm of coefficients in (12) (a) and (c) when noise is simultaneously added to ω_0 and $u(t)$; (b) and (d) for the noise-free case, see Fig. 10. The floor in (a) and (b) is at the order of 10^{-3}; (c) and (d) are the 2D top views of (a) and (b), respectively.

The analysis of the presented noisy scenarios shows that using the non reductionist model for PLL models is compatible with Viterbi's seminal work [20] that has been used for practical design situations [21]. A modern view of the problem, as discussed in [22], can be considerably improved when phase reduction approach is replace by the non reductionist one.

5 Conclusions

The main contribution presented is the formulation of the PLL problem in a non reductionist way, differently from the traditional phase reduction approach, by using a dynamic state-space model.

The reductionist model should be used for analysis whereas the non-reductionist approach should be preferred for more realistic simulations and to make design decisions which do not rely on the hypotheses underlying the reductionist model that are not verified in practice. The proposed model, unlike the reductionist one, i) takes into account the nonlinearity of the sine function, since the model remains valid for large phase errors; ii) does not assume the filter is ideal; iii) enables simulating and
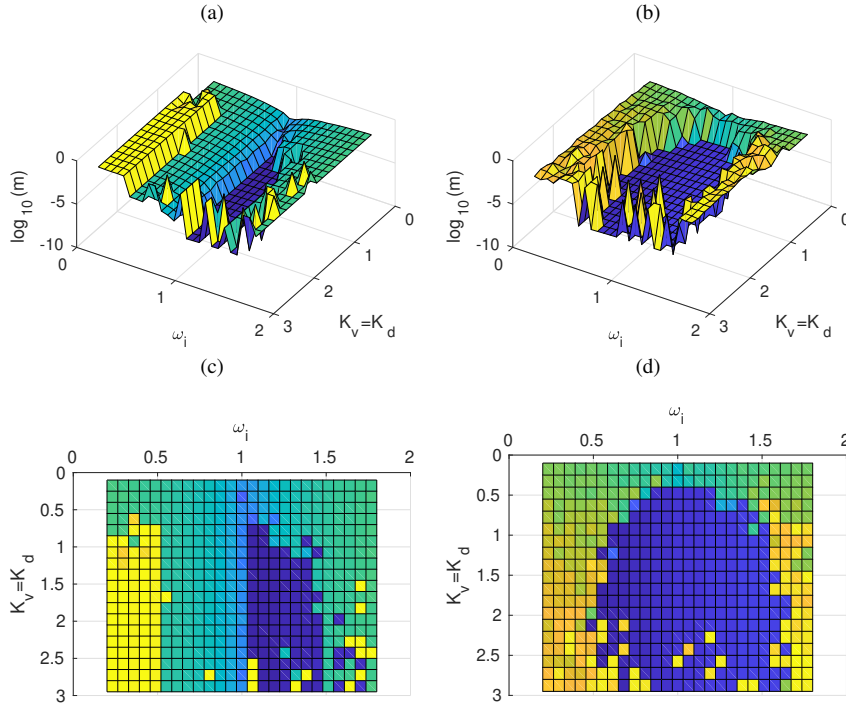
Fig. 16 Logarithm of coefficients in (12) (a) and (c) when noise is simultaneously added to ω_0 and $u(t)$; (b) and (d) for the noise-free case, see Fig. 11. The floor in (a) and (b) is at the order of 10^{-5}; (c) and (d) are the 2D top views of (a) and (b), respectively.

investigation of noisy scenarios; iv) enables simulating different VCO configurations with ease, as in (9).

Therefore with the proposed model friendly numerical analysis can be performed, providing an accurate view of the capture and lock-in ranges observing regions and boundaries in performance diagrams.

By comparison with studies reported in the literature in seems that abrupt transitions in the performance diagrams are closely related to bifurcations obtained using reductionist models that include second-order harmonics.

Consequently, according to the input signal characteristics, bounds for gain parameters adjustments can be easily visualized, even considering noise effects either in the VCO central frequency or in the input signal.

Measures of synchronization performance were defined (Sec. 3), allowing to provide criteria to choose gain PLL parameters and, consequently, to set the capture and lock-in ranges, as shown by examples, operationally important when a clock distribution network with PLL nodes must be built.

Extensive simulations that consider noise in both the VCO central frequency and in the input signal show that the state-space model is consistent with some basic features reported in the literature, such as overall performance when second-order
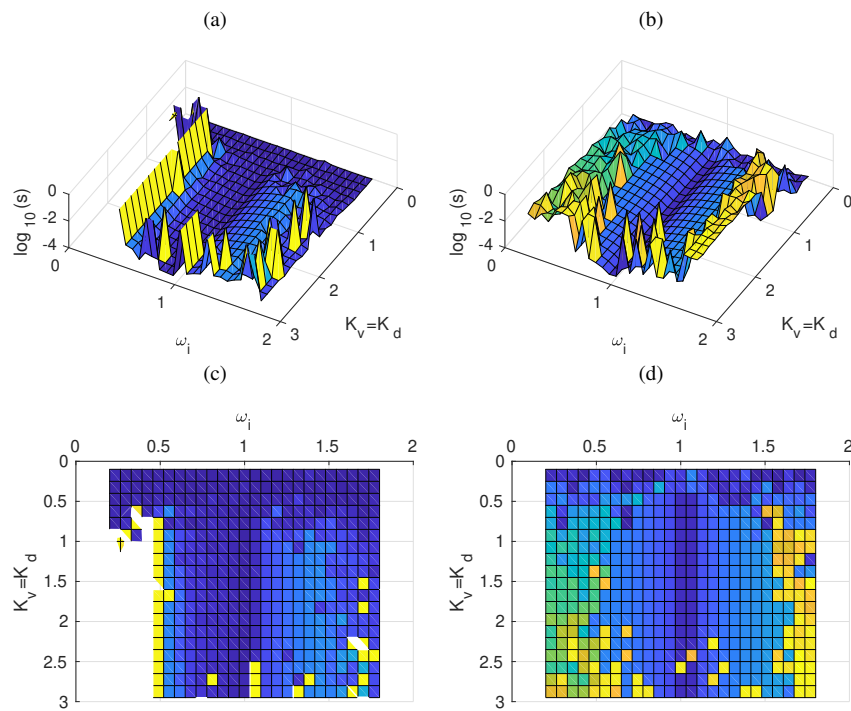
Fig. 17 Logarithm of coefficients in (12) (a) and (c) when noise is simultaneously added to ω_0 and $u(t)$; (b) and (d) for the noise-free case, see Fig. 12. The floor in (a) and (b) is at the order of $10^{-3.5}$; (c) and (d) are the 2D top views of (a) and (b), respectively.

harmonics are not assumed absent [14], and the pass-band filtering properties of PLLs [4].

In view of the appealing features of the proposed state-space model, the next step is to investigate its use in the analysis and design of PLL networks that are typical in GPS-positioning applications [24].

Declaration of competing interest

The authors declare that they have no known competing financial interests or personal relationships that could have appeared to influence the work reported in this paper

Acknowledgments

References

1. de Bellescize H., La reception synchrone L'Onde electrique, changed to revue de l'electricité et de l'electronique, vol. 11 (1932), pp. 230-240

2. Staszewski R.B., Balsara P.T., Phase-domain all-digital phase-locked loop IEEE Transactions on Circuits and Systems II, Exp Briefs, 52 (3) (2005), pp. 159-163

3. Alvarez M.A., Spagnolini U., Distributed time and carrier frequency synchronization for dense wireless networks, IEEE Transactions on Signal and Information Processing over Networks, 4 (4) (2018), pp. 683-696.

4. Lindsey W.C. Synchronization systems in communication and control (1st ed), Prentice Hall, Engiewood Cliffs, NJ: USA (1972)

5. Gersho A., Karafin B.J., Mutual synchronization of geographically separated oscillators Bell System Technical Journal (1966), pp. 1689-1703.

6. Brilliant M.B., The determination of frequency in systems of mutually synchronized oscillators, Bell System Technical Journal (1966), pp. 1737-1748.

7. Bregni S. A historical perspective on telecommunications network synchronization, IEEE Communications Magazine, 36 (6) (1998), pp. 158-166.

8. Bregni S. Synchronization of digital telecommunications networks, (1st ed), John Wiley & Sons, Ltd., West Sussex-UK (2002)

9. Best R.E. Phase-locked loops (6th ed), McGraw Hill, New York (2007)

10. Piqueira J.R.C., de Godoi A.C.B., Clock signal distribution with second order nodes: Design hints ISA Transactions, 115(2021), pp. 124-142

11. Dandapathak M., Chakraborty S., Studies on of phase error oscillations in a class of third-order optical phase locked loop and its effect on a slave optical phase locked loop, Optical Engineering, 61(6) (2022), pp. 066101-2–066101-20

12. Piqueira J.R.C., Hopf bifurcation and chaos in a third-order phase-locked loop, Communications in Nonlinear Science and Numerical Simulation, 42 (2017), pp. 178-186.

13. Nakao H., Phase reduction approach to synchronisation of nonlinear oscillators, Contemporary Physics 57(2016), pp. 188-214.

14. Piqueira, J.R.C., Monteiro, L.H.A., Considering second-harmonic terms in the operation of the phase detector for second-order phase-locked loop, IEEE Transactions on Circuits and Systems I, v. 50(2003), pp. 805-809, 2003.

15. Hsieh, G. C. and Hung, J. C. Phase-locked loop techniques - a survey. IEEE Transactions on Industrial Electronics, 43(6) (1996), pp. 609-615.

16. Osipov, G. V., Kurths, J., and Zhou, C., Synchronization in Oscillatory Networks, Springer, Berlin (2007).

17. Leonov G.A., Kuznetsov N.V., Yuldashev M.V., Yuldashev R.V., Hold-in, pull-in, and lock-in ranges of PLL circuits: Rigorous mathematical definitions and limitations of classical theory, IEEE Transactions on Circuits and Systems I: Regular Papers, 62 (10) (2015), pp. 2454-2464.

18. Piqueira, J. R. C., Using bifurcations in the determination of lock in ranges for third-order phase-locked loops, Communications in Nonlinear Science Numerical Simulation, 14 (5) (2009), pp. 2328–2335. (https://doi.org/10.1016/j.cnsns.2008.06.012)
19. Clusella P., Politi A., Noise-induced stabilization of collective dynamics, Physical Review E 95(2017), 062221.
20. A. Viterbi, Phase-Locked Loop Dynamics in the Presence of Noise by Fokker-Planck Techniques, Proceedings of the IEEE, 12 (1963), pp. 1737-1753.
21. Xu, X., Huihua, L., Ao, S., Design of low phase noise and fast locking PLL frequency synthesizer, 2011 International Conference on Electric Information and Control Engineering, ICEICE 2011 - Proceedings, pp. 4113 - 4116, International Conference on Electric Information and Control Engineering (2011). (DOI: 10.1109/ICEICE.2011.5777391)
22. Ripani, B., Modenini, A., Montorsifellow, G., Digital PLLs for Phase Noise Channels: A Concept Based on the Tikhonov Distribution, IEEE Signal Processing Letters, 31(2024), pp. 2040 - 2044. (DOI: 10.1109/LSP.2024.3432048)
23. Rosenblum, M. G., Pikovsky, A. S., and Kurths, J., Phase synchronization of chaotic oscillators, Physical Review Letters, 76(11)(1996), pp. 1804-1807.
24. Moschas, F., Stiros, S., PLL bandwidth and noise in 100 Hz GPS measurements, GPS Solutions, 19(2015), pp. 173–185.